Chapter

Optical Study of Porous Silicon Layers Produced Electrochemically for Photovoltaic Application

Rahmouni Salah

Abstract

In previous years, porous silicon is rapidly attracting increasing interest in various fields and has received a great deal of attention from researchers because of its potential use in a variety of industrial applications such as photovoltaic device applications. The present study conclusively suggested that in order to prepare porous silicon samples, we need to determine the optimal conditions that lead to the increase of the optical efficiency. Porous silicon layers were elaborated by the electrochemical etching method using doped *p*-type ⟨100⟩-oriented silicon substrate. The photoluminescence (PL) and the spectroscopic ellipsometry (SE) measurements were used to calculate the physical and optical parameters (porosity, thickness) (refractive index and extinction coefficient). This study can give a very important interest in the photovoltaic field.

Keywords: porous silicon, antireflective coating, electrochemical anodization, photoluminescence, spectroscopic ellipsometry

1. Introduction

Porous silicon has undergone many developments; it has a very wide field of application and has received a great deal of attention from researchers because of its potential use in a variety of industrial applications such as photovoltaic device applications [1–4], chemical and gas sensors [5–12], biosensors [13, 14], biomedical applications [15], micromachining [16–18], templates for micro- and nanofabrication [19–21], and solar cells and photoluminescence [1, 22, 23]. However, a very limited data of optoelectronic uses in this field are available [24, 25]. It is reported that the photoluminescence of porous silicon (PS) has achieved a large-scale investigation, giving an explanation of the photoluminescence phenomenon with obtaining the optical properties of porous silicon, as well as determining its refractive index and the gap energy, which can be determined directly by the absorption measurement, or by a non-destructive technique called spectroscopic ellipsometry (SE).

However, the physical and optical properties could be studied. In addition, some of the physical phenomena are still poorly understood because of the strong relationship between the PS nanostructure and the elaboration conditions (HF concentration,

current density, and anodization time) [26]. The present study conclusively suggested that in order to prepare porous silicon samples, we need to determine the optimal conditions that lead to increase the optical efficiency. Herein, we need to study the correlation between the results extracted from the PL analysis and those obtained by ellipsometry. The study of the evolution of the intensities of the emission spectra obtained by the measurement of PL as a function of the porosity and the thickness determined by the ellipsometry of the layers for silicon substrates oriented P-100 of low resistivity is made to precisely clarify the evolution of optical parameters.

2. Photoluminescence study

The PL measurements were carried out by a solid laser 447 nm and detected through a Jobin Yvon 250-mm HR mono-chromator, with a GaAs photomultiplier associated to standard lock-in technique. Of note, the laser power of 7.66 mW was applied on the surface of the sample.

The optical characterization used in our work is based on "the radiation-matter interaction"; it tells us about the optical properties of the material. Photoluminescence spectroscopy is widely used to study the electronic structure of materials and the processes of radiative recombinations. It is a nondestructive optical characterization technique for nanomaterials.

In this part, using photoluminescence (PL) spectroscopy, we will determine the optical properties of porous silicon samples produced by electrochemical anodization. First, we analyze the PL spectra of SiP at room temperature. Second, we study the variation of the intensity, and the integrated intensity of PL in the temperature range [10–300 K].

2.1 Experimental details

Serial of porous silicon samples were prepared of *p*-type (100)-oriented silicon substrate with a resistivity of 0.001–0.02 Ω cm.

The experimental set-up consists first of all of a pulsed laser, the emission wavelength of which can be changed. The laser we have allows us to take measurements with an excitation of 447 nm. The laser beam is then conveyed to the sample by sets of mirrors. The sample is on a sample holder that can be placed in a cryostat (for low temperature studies) (**Figure 1**).

Figure 1.
Experimental device used for the measurement of photoluminescence.

2.2 Photoluminescence of porous silicon layers

2.2.1 Evolution of photoluminescence spectra of P-type porous silicon prepared at different etching time

All of the PS samples showed a visible PL at a room temperature. **Figure 2** illustrates the PL spectra of samples of p-type elaborated at different etching times (60, 120, 180, and 240 s) as well as an etching current density of 15 mA/cm^2.

Figure 2 shows that the observed large band, that ranges from 550 to 780 nm, decreases in time with a peak of 668 nm, and a decreased full width at half maximum (FWHM) from 226 to 112 is obtained along with an increase of PL intensity from 0.07 to 21.06.

The width of this PL band is attributed to the wide size distribution of the silicon nanocrystallites which constitute the porous layer. The intense spectrum is characterized by a maximum at the energy of 1.86 eV and a width at mid-height of the order of 112 meV.

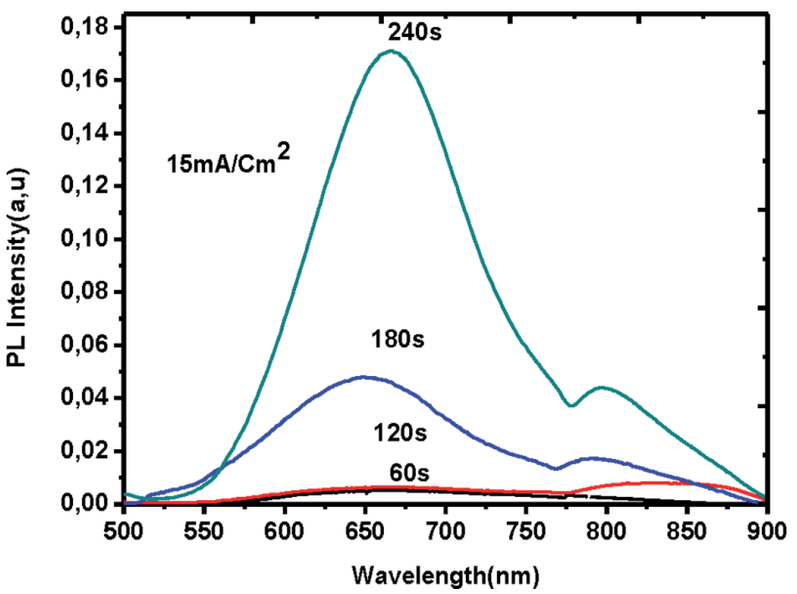

Figure 2.
Evolution of photoluminescence spectra of P-type porous silicon prepared at different etching times.

In addition, we noticed a second less intense band compared to the first. This may be due to an oxide layer located in a band between 780 and 900 nm (**Table 1**).

Samples	Etching time (s)	λPic (nm)	FWHM (meV)	IPLMax (u,a)	Eg (eV)
S1	60	628	226	0.07	1.96
S2	120	666	189	0.89	1.86
S3	180	652	122	6.81	1.91
S4	240	668	112	21.06	1.86

Table 1.
Optimized fitting parameters corresponding to the theoretical curves of porous silicon samples prepared at different etching time and current density of 15 mA/cm^2.

Figure 3 shows the variation of the PL intensity and the width at half height (FWHM) as a function of the anodization time.

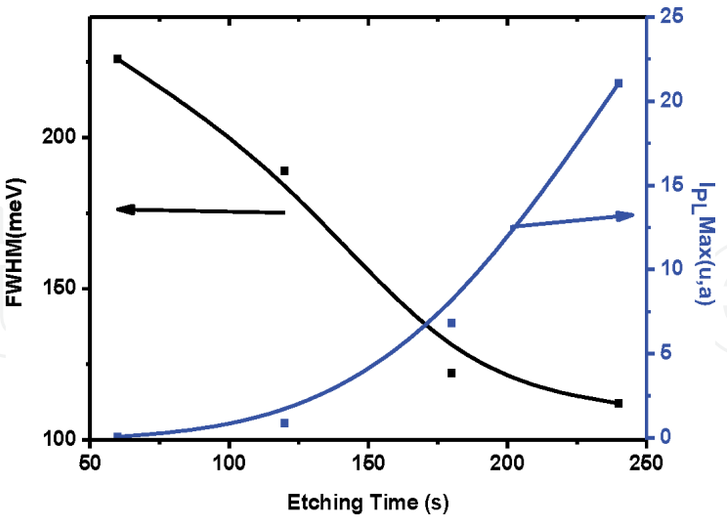

Figure 3.
The variation of the intensity, PL, and the width at half height (FWHM) as a function of the anodization time.

From **Figure 3**, we notice that the width at half height of the PL spectra decreases as a function of the anodization time. As known the thickness of the porous layer increases as a function of the anodization time, then deduces that the width at half height decreases, and the intensity of PL increases as a function of the thickness of the porous layer. This is due to the decrease in the sizes of nano-crystallites. However, note that the intensity of PL increases as a function of the anodization time.

2.2.2 Evolution of photoluminescence spectra as a function of the anodization current density

Figure 4 shows the PL spectra of p-type samples that were obtained from different etching current densities, 5, 10, 15 and 20 mA/cm^2, and etching time of 180 s. The presented serial in **Figure 1** indicates near similar variations of the PL

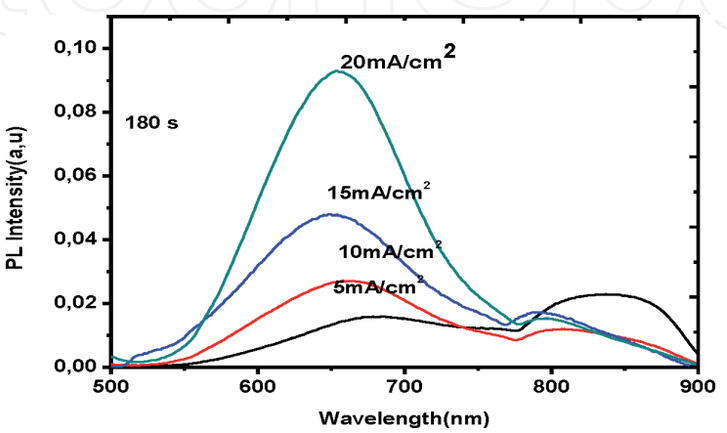

Figure 4.
Evolution of photoluminescence spectra of P-type porous layers prepared at different etching current density.

intensity. However, a remarkable increase of the PL intensity ranges from 2.59 to 11.72 was noticed (**Table 2**).

The two spectra show an improvement in the PL intensity as a function of etching current density and etching time. On the other hand, we noticed that the PL intensity reached the maximum value of JCM, that equals 20 mA/cm^2, with tm = 240 s. The slight blue-shift energy of PL band allow us to attribute a confinement of more and more wells and wire that leads to diminution of nanocrystallite size [27, 28].

The porous layer obtained from p-type silicon wafer is presented as cylindrical and spherical crystallites [29, 30]. Therefore, PS is defined as a mixture of quantum wells (QWs) and quantum wire following different concentrations and sizes. In the case of the increased etching time, the thickness of porous silicon layer increases from 106.3 to 1027.2 nm (**Table 3**).

Figure 5 shows the variation of the PL intensity and the width at half height (FWHM) as a function of the anodization current density.

The width at half height (FWHM) decreases according to the current density; this is due to the increase in porosity, therefore the increase in the intensity of PL.

Figure 6 depicts that the thickness and the integral intensity of the PL increase as function of etching time, meanwhile the porosity and the integral intensity of PL increase as a function of the current density **Figure 7**. On the other hand, the PL intensity of the porous layer increases as a function of etching time and current density.

Samples	Current density (mA/Cm2)	λPeak (nm)	FWHM (meV)	IPLMax (u,a)	Eg (eV)
S5	5	682	249	2.59	1.81
S6	10	665	210	4.12	1.87
S7	15	652	122	6.81	1.91
S8	20	655	111	11.72	1.90

Table 2.
Optimized fitting parameters corresponding to the theoretical curves of porous silicon samples prepared at different etching current densities and etching time of 180 s.

Samples	Etching time (s)	Current density (mA/Cm^2)	Thickness (μm) (d)	Porosity (%) (P)	n	k
S1	60	15	0.1063	36.02	/	/
S2	120	15	0.7061	58.84	/	/
S3	180	15	0.9058	70.20	/	/
S4	240	15	1.0272	76.89	/	/
S5	180	5	0.0985	34.53	1.77	0.0035
S6	180	10	0.7221	61.45	1.43	0.0022
S7	180	15	0.9058	70.20	1.33	0.0018
S8	180	20	1.0311	78.23	1.22	0.0014

Table 3.
Different parameters evaluated from the optical model of samples obtained at different etching times and different current densities [31].

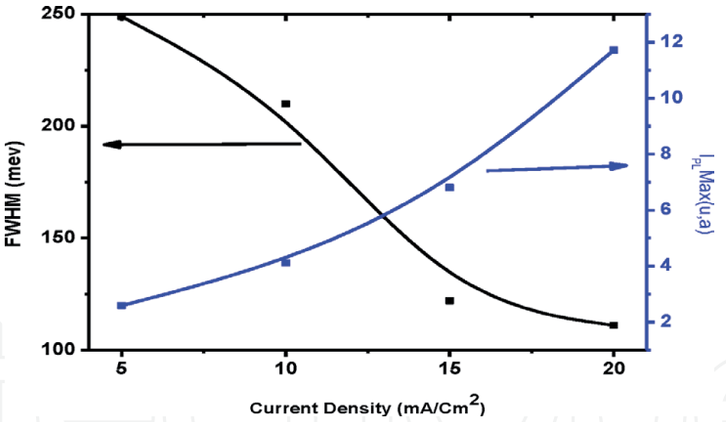

Figure 5.
The variation of the PL intensity and the width at half-height (FWHM) as a function of the anodization current density.

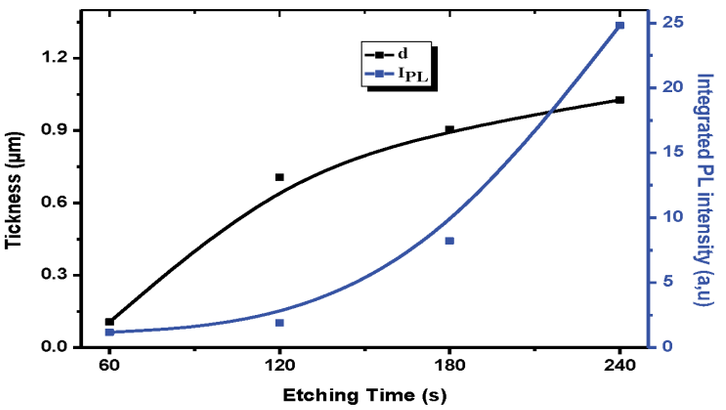

Figure 6.
Variation of thickness and integrated PL intensity according to etching time [31].

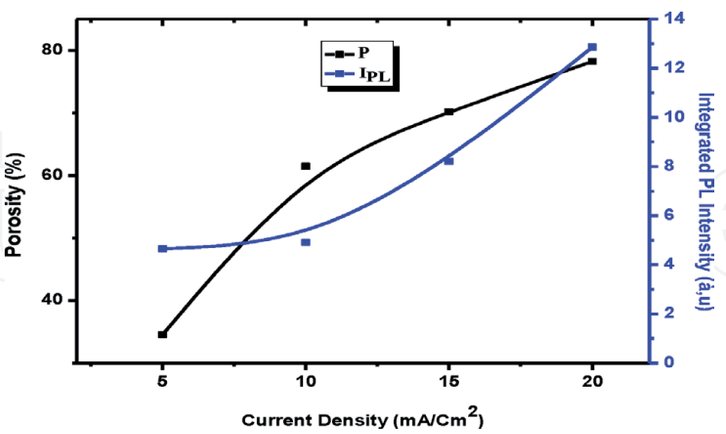

Figure 7.
Variation of porosity and integrated PL intensity according to etching current [31].

2.3 Study of low temperature photoluminescence

This part is devoted to the study of the evolution of the PL band as a function of temperature in order to identify the nature of the energy levels which are at the origin of this PL and to understand the mechanisms of radiative recombinations which participate in this PL. We have studied the variation of intensity and the integrated intensity all as a function of temperature in the range [10–300 K].

The sample studied is of type N (100), produced under these conditions: [HF] = 16%, t = 3 min and j = 20 mA/cm^2.

2.3.1 Evolution of PL intensities as a function of temperature

i. At low temperatures (T < 50 K), the decrease in IPL as a function of the increase in temperature is attributed to the transfer of excitons to states of lower energies in a non-radiative manner by thermal activation (**Figure 8**).

ii. While increasing the intensity of PL in the temperature range of (50 K ≤ T ≤ 80 K) indicates that the excitons are trapped in the lower localized states are thermally activated toward the higher states and then recombine radiatively and generate an increase in IPL intensity [32].

iii. At higher temperatures (T ≥ 80 K), thermal activation becomes more dominant and localized excitons become free and can diffuse in a non-radiative manner in the structure leading to a decrease in the intensity of PL [32].

iv. In the same figure, we notice the appearance of an intensity peak of PL at a characteristic temperature T_M = 80 K.

2.3.2 The intensity of PL as a function of the inverse of temperature

According to Zhao et al. and Weng et al., there are two types of transfer processes:

i. The first is a tunnel transfer [33, 34].

ii. The second is transfer by thermal dissociation [34] which is negligible at low temperatures.

But we have shown that the variation in the intensity of PL with temperature is due to the presence of these two exciton injection processes.

Ten et al. have shown that the increase in temperature could increase the tunneling process [35]. However, Hua et al. confirm that thermal dissociation of excitons increases with temperature, which favors the leakage of excitons from Q_{Ds} to Q_{Ws} at lower energy levels [36]. In **Figure 9**, we represent the integrated

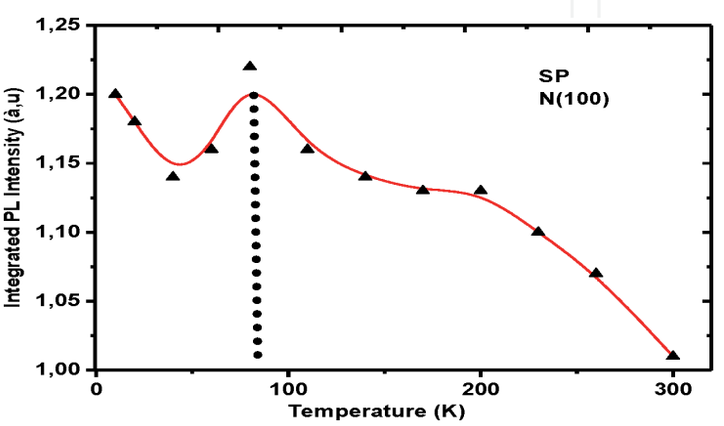

Figure 8.
Evolution of PL intensities as a function of the temperature of a SiP layer produced on an N-type substrate (100).

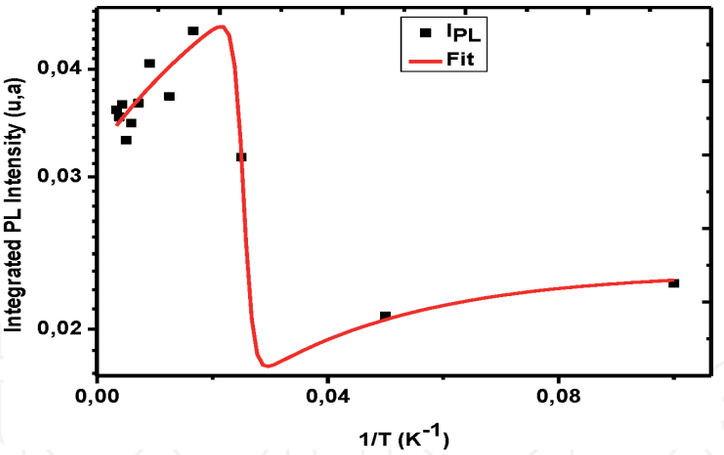

Figure 9.
Variation of the integrated intensity of PL as a function of the inverse of the temperature.

IPL	0.0232
a1	0.4046
e1	36.6044*8.33E-5 = 3.05 meV
A	1.7293
e2	1205.8422*8.33E-5 = 100.44 meV
a2	1.1545E13

Table 4.
The values obtained from the parameters of the equation.

intensity of PL as a function of the inverse of the temperature. Taking into account these two transfer processes, we fitted the experimental curve using the two-energy model, this empirical model is presented in Eq. (1) below [37]:

$$I_{PL}(T) = \frac{I_{PL}(0)}{\left[1 + a_1 \exp\left(-\frac{e_1}{kT}\right)\right]^2} \times \left(1 + \frac{A}{\left[1 + \frac{1}{a_2} \times \exp\left(\frac{e_2}{kT}\right)\right]}\right) \quad (1)$$

where e_1: first thermal activation energy; e_2: second thermal activation energy; A, a_1 and a_2: the fixing parameters; and I_{PL}: the intensity PL.

The different values found are presented in **Table 4**.

From the results, it can be seen that the thermal activation energy of one energy level is different from that of another level. This phenomenon can be explained by the increase in the Tunnel process with the increase in temperature [35]. We can also know the thermal activation energy of phonons in porous silicon.

3. Ellipsometric spectroscopy measurement

Spectroscopic ellipsometry is a very sensitive optical surface analysis method that allows the physical and morphological properties of a flat sample to be probed at different scales and at different energies. It has experienced significant growth over the past 100 years [38] and particularly over the past 20 years with modern computing. The

technique makes it possible to obtain information on the surface of a massive sample, on the volume of a thin film or even on the interfaces. Ellipsometry has the advantage of being very simple and quick to implement, nondestructive, of allowing in-situ and real-time monitoring, and being applicable to a very wide range of samples.

3.1 Expérimental details

Ellipsometric measurements were performed on the porous silicon substrate for an angle of incidence of 78° in the spectral range 250–2000 nm using the GES5 Sopra made rotating polarizer spectroscopic ellipsometer was used for the (SE) spectroscopic ellipsometry measurement, controlled by the WinElli-II software.

To extract the thickness of the PS layer from measuring of SE, an optical model must be assumed, as well as the calculated data have to follow experimental spectra. In applying EMA software, we utilized a model of a multi-layer model, whereas the first mixture of the layer (void/SiO_2), while the second layer is (Sic/void), As indicated in **Figure 10**, a high improvement in the fit quality was observed [31].

3.2 Experimental device used

Figure 11 shows the "GES5" spectroscopic ellipsometer used in our work; this ellipsometer is assisted by a computer and controlled by the WinElli-II software.

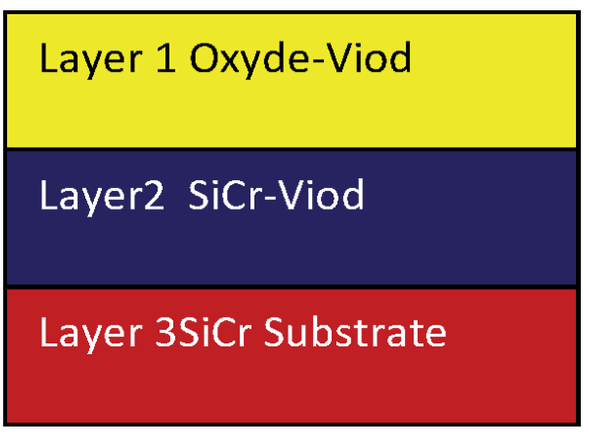

Figure 10.
The multilayer model of the PSL [31].

Figure 11.
Real photo of the GES 5 Sopra Ellipsometry used in our work.

This work was carried out at the techno pole photovoltaic laboratory of bordj çedria in Tunisia.

3.3 Thickness measurement

We measured the thicknesses of the series A samples (see **Table 1**).
Figures 12 and **13**, respectively, represent the ellipsometric spectra of samples S2 and S3.

The measure and the shape of the ellipsometrical spectra are presented in **Figures 12** and **13**.

The first serial allows us to determine ellipsometry. The adjustment parameters for the thickness of separated layers, using each sub-layer of the optical model are summarized in **Table 3**.

Figure 6 shows an agreement between the PL measurement presented by the integral intensity of PL along with the SE measurement presented by the thickness of porous layers obtained through varying etching time.

3.4 Porosity measurement

The second serial of samples was obtained following an etching time of 180 s and a current density varying from 5 to 20 mA/cm^2. **Figures 14** and **15** show the measurement and the shape of ellipsomety spectra.

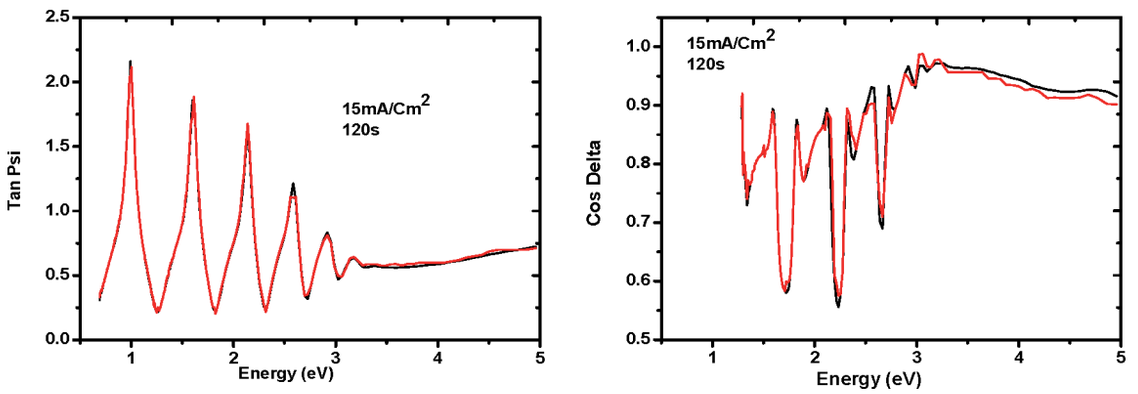

Figure 12.
SE measurements of the PSL obtained by using 15 mA/cm^2, 120 s, and the calculated spectra based on the best-fitted parameters [31].

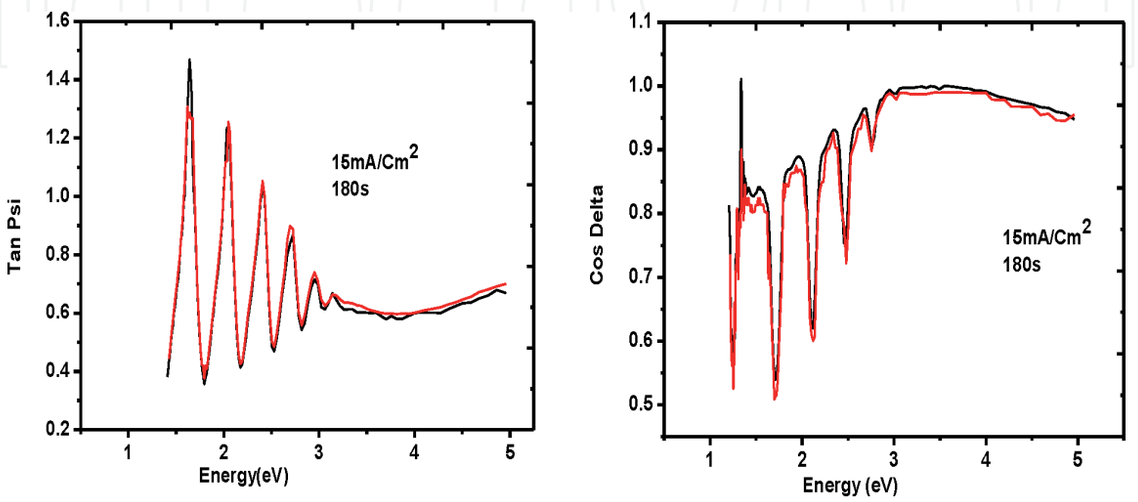

Figure 13.
SE measurements of the PSL obtained by using 15 mA/cm^2, 180 s, and the calculated spectra based on the best-fitted parameters [31].

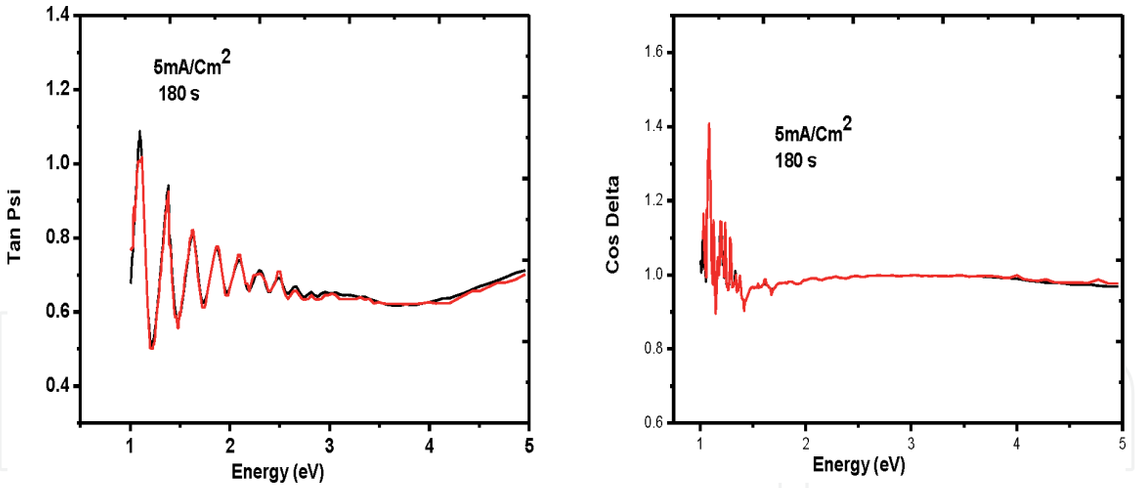

Figure 14.
SE measurements of the PSL obtained in using 5 mA/cm², 180 s, and the calculated spectra based on the best-fitted parameters [31].

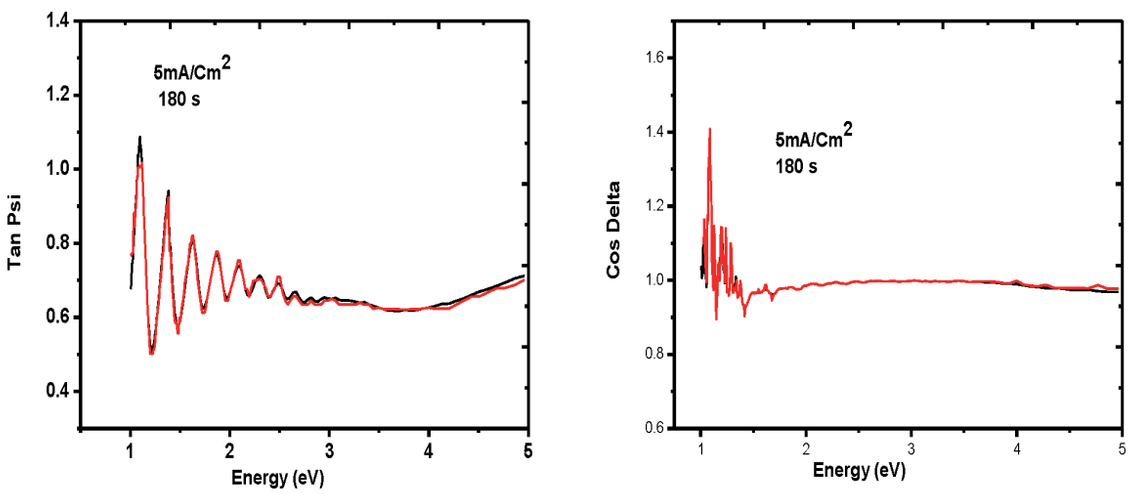

Figure 15.
SE measurements of the PSL obtained in using 10 mA/cm², 180 s, and the calculated spectra based on the best-fitted parameters [31].

The second serial allows us to determine the porosity of separated layers, using ellipsometrical method. The adjustment parameters for each sub-layer of an optical model are summarized in **Table 3**.

Figures 14 and **15**, respectively, show the measurement and shape of the spectra obtained by ellipsometry, the porous layers (S5, S6) obtained by J = 5 mA/cm2 and J = 10 mA/cm2, and an anodization time of 180 s.

Figure 7 shows an agreement between the PL measurement presented by the integral intensity of PL and SE measurements presented by the porosity of porous layers obtained following varying current density.

The two produced curves using values obtained by ellipsometry show that the thickness is as an increased function following etching time; meanwhile the porosity is as an increased function following the current density [39].

In this case, the PL comportment can be explained by the absence of the laser interference in the cleaned layer, as previously indicated. The contrary case was noticed in the thickness and the porous layer of silicon variations.

Adjusting the parameters of the proposed model to the experimental measurements taken on the sample, allowed us to obtain the values presented in **Table 3**.

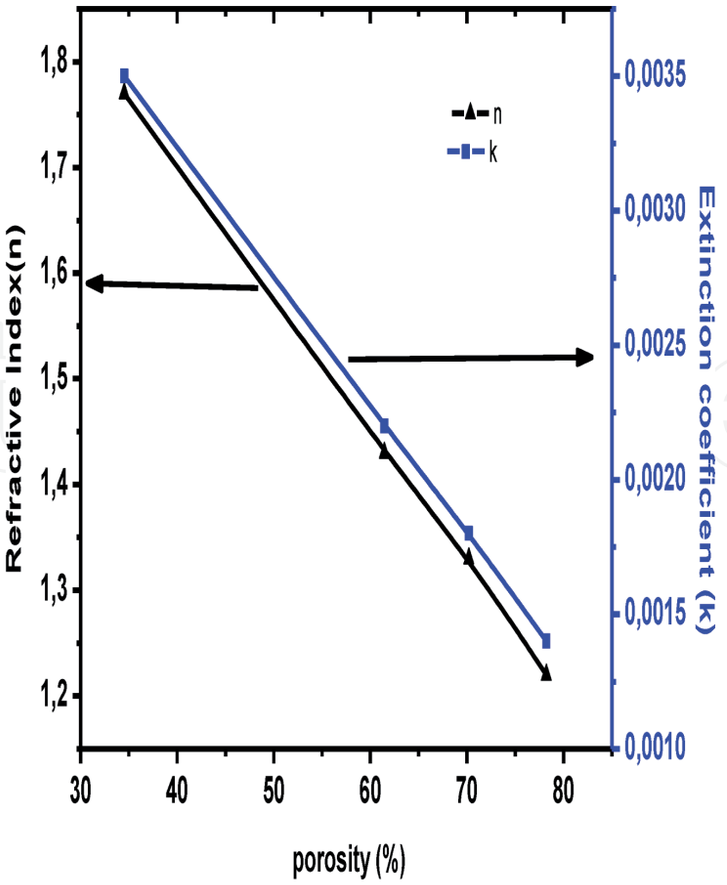

Figure 16.
Variation of refractive index and extinction coefficient as a function of porosity [31].

3.5 Calculation of the refractive index (n) and the extinction coefficient (k)

The results illustrated in **Table 3** and **Figure 16** show that the refractive index and the extinction coefficient are as a decreased function along with the porosity.

In case of a porosity of 34%, we get n = 1.77 and k = 0.0035, while for porosity of 78%, we get n = 1.22 and k = 0.0014 [31].

This result shows that the remained porous layer is more proper, but less thick and gives us a best PL intensity. Hence, the laser diffuses in wells by confinement effect. This confinement means to confine the incident laser radiation in crystallites seals and therefore the laser reflection is reduced following the big values of thickness and the porous layers.

4. Conclusion

In this study, we developed porous silicon layers by electrochemical anodization, the optical characterization made by spectroscopic ellipsometry (SE), and photoluminescence (PL); this characterization enabled us to calculate the physical and optical parameters (porosity, thickness; refractive index, extinction coefficient). To determine the effect of the etching parameters, we have suggested that for a good elaboration of the porous layers, it would be necessary to know the optimal conditions of anodization, taking into account the great role of the oxide layer on the surface. We note that the results obtained demonstrate that it excites a correlation between photoluminescence characterization (PL) and measurement of spectroscopic ellipsometry (SE), and these results are very important in the photovoltaic field.

Author details

Rahmouni Salah[1,2]

1 Higher School for Professor of Technological Education, ENSET, Skikda, Algeria

2 Laboratory of Physical Chemistry and Biology of Materials (LPCBM), ENSET, Skikda, Algeria

*Address all correspondence to: rahmouni.eln@gmail.com

References

[1] Ramirez A, Aziz WJ, Hassan Z, Omar K, Ibrahim K. Improved performance of solar cell based on porous silicon surfaces. Optik-International Journal for Light and Electron Optics. 2011;**122**(23):2075-2077

[2] Mohamed BA, Anouar H, Brahim B. Improvement of multicrystalline silicon solar cell performance via chemical vapor etching method-based porous silicon nanostructures. Solar Energy. 2012;**86**(5):1411-1415

[3] Sanchez de la Morena S, Recio-Sanchez G, Torres-Costa V, Martin-Palma RJ. Hybrid gold/porous silicon thin films for plasmonic solar cells. Scripta Materialia. 2014;**74**:33

[4] Atyaoui M, Dimassi W, Atyaoui A, Elyagoubi J, Ouertani R, Ezzaouia H. Improvement in photovoltaic properties of silicon solar cells with a doped porous silicon layer with rare earth (Ce, La) as antireflection coatings. Journal of Luminescence. 2013;**141**:1-5

[5] Harraz FA, Ismail AA, Bouzid H, Al-Sayari SA, Al-Hajry A, Al-Assiri MS. A capacitive chemical sensor based on porous silicon for detection of polar and non-polar organic solvents. Applied Surface Science. 2014;**307**:704-711

[6] Bardaoui A, Chtourou R, Amlouk M. Hand book, porous silicon multilayers: Synthesis and applications. Nova Science Publishers; 2012

[7] Salem MS, Sailor MJ, Harraz FA, Sakka T, Ogata YH. Electrochemical stabilization of porous silicon multilayers for sensing various chemical compounds. Journal of Applied Physics. 2006;**100**(8):083520

[8] Karthik TVK, Martinez L, Agarwal V. Porous silicon ZnO/SnO_2 structures for CO_2 detection. Journal of Alloys and Compounds. 2018;**731**:853

[9] Salem MS, Sailor MJ, Harraz FA, Sakka I, Ogata YH. Sensing of chemical vapor using a porous multilayer prepared from lightly doped silicon. Physica Status Solidi C. 2007;**4**(6):2073-2077

[10] Li M, Hu M, Zeng P, Ma S, Yan W, Qin Y. Effect of etching current density on microstructure and NH_3-sensing properties of porous silicon with intermediate-sized pores. Electrochimica Acta. 2013;**108**:167-174

[11] Dwivedi P, Das SD. Synthesized MoS_2/Porous Silicon Nanostructures for Efficient and Selective Ethanol Sensing at Room Temperature. ACS Applied Materials & Interfaces. 2017;**9**(24):21017-21024

[12] Harraz FA, Ismail AA, Bouzid H, Al-Sayari SA, Al-Hajry A, Al-Assiri MS. Mesoporous silicon layer as a highly sensitive ethanol sensor. International Journal of Electrochemical Science. 2014;**9**:2149-2157

[13] Myndrul V, Viter R, Savchuk M, Shpyrka N, Erts D, Jevdokimovs D, et al. Porous silicon based photoluminescence immunosensor for rapid and highly-sensitive detection of Ochratoxin A. Biosensors and Bioelectronics. 2018;**102**:661-667

[14] Harrez FA. Porous silicon chemical sensors and biosensors: A review. Sensors and Actuators B: Chemical. 2014;**202**:897-912

[15] Sarkar T, Basu D, Mukherjee N, Das J. Comparison of glucose sensitivity of nano and macro porous silicon. Materials Today - ScienceDirect. 2018;**5**(3) Part 3:9798

[16] Sun X, Parish G, Keating A. Micromachined microbeams made from porous silicon for dynamic and static mode sensing. Sensors and Actuators, A: Physical. 2018;**269**:91-98

[17] Wallace RA, Sepaniak MJ, Lavrik NV, Datskos PG. Evaluation of porous silicon oxide on silicon microcantilevers for sensitive detection of gaseous HF. Analytical Chemistry. 2017;**89**(11):6272-6276

[18] Lysenko V, Perichon S, Remaki B, Barbier D. Thermal isolation in microsystems with porous silicon. Sensors and Actuators A. 2002;**99**:13-24

[19] Jia C, He S, Song J, Jin Y, Zhu W, Cheng Q. Fabrication of micro/mesoporous silica tubes templated by electrospun cellulose acetate fibers. Cellulose Chemistry and Technology. 2017;**51**(7-8):693-701

[20] Bandarenka HV, Girel V, Zavatski SA, Panarin A, Terekhov SN. Progress in the development of SERS-active substrates based on metal-coated porous silicon. Materials. 2018;**11**(5):852

[21] Harraz FA. Impregnation of porous silicon with conducting polymers. Physica Status Solidi C. 2011;**8**(6):1883-1887

[22] Lenshin AS, Seredin PV, Kashkarov VM, Minakov DA. Origins of photoluminescence degradation in porous silicon under irradiation and the way of its elimination. Materials Science in Semiconductor Processing. 2017;**64**:71-76

[23] Omar K, Salman KA. Effects of electrochemical etching time on the performance of porous silicon solar cells on crystalline n-type (100) and (111). Journal of Nanoparticle Research. 2017;**46**:45-46

[24] Mazzoleni C, Pavesi L. Application to optical components of dielectric porous silicon multilayers. Applied Physics Letters. 1995;**67**(20):2983-2985

[25] Hadi HA, Ismail RA, Habubi NF. Optoelectronic properties of porous silicon heterojunction photodetector. Indian Journal of Physics. 2014;**88**(1):59-63

[26] Ji J-M, He X-X, Duan Q, Wang Z-X. Preparation of porous silicon substrate for protein microarray fabrication by double-cell electrochemical etching method. Chinese Journal of Analytical Chemistry. 2013;**41**(5):698-703

[27] Ee DTJ, Sheng CK. MIN Isa. photoluminescence of porous silicon prepared by chemical etching method. The Malaysian Journal of Analytical Sciences. 2011;**15**(2):227-231

[28] Gelloz B. Possible explanation of the contradictory results on the porous silicon photoluminescence evolution after low temperature treatments. Applied Surface Science. 1997;**108**(4):449-454

[29] Cullis AG, Canham LT, Dosser OD. The structure of porous silicon revealed by electron microscopy materials. Research Society Symposium Proceedings. 1992;**256**(7)

[30] Berbezier I, Halimaoui A. A microstructural study of porous silicon. Journal of Applied Physics. 1993;**74**(9):5421

[31] Rahmouni S, Zighed L, Chaguetmi S, Daoudi M, Khelifa M, Karyaoui M, et al. Correlation between photoluminescence and ellipsometric measurements of porous silicon layers. Optoelectronics and Advanced Materials. 2018;**12**(9-10):5535-5558

[32] Mabrouk A et al. Correlation between optical properties surface morphology of porous silicon electrodeposited by Fe^{3+} ion. Superlattices and Microstructures, Elsevier. 2015;**77**:219-231

[33] Weng GE, Zhang BP, Liang MM, Lv XQ, Zhang JY, Ying LY, et al. Optical properties and carrier dynamics in asymetric coupled InGasN multiple

quantum wells. Materials Letters. 2013;**6**:2

[34] Zhao D, Li B, Wu C, Lu Y, Shen D, Zhang J, et al. Temperature dependence of carrier transfer and exciton localization in ZnO/MgZnO heterostructure. Journal of Luminescence. 2006;**119-120**:304-308

[35] Ten S, Henneberger F, Rab M, Peyghambarian N. Femtosecond study of exciton tunneling in (Zn,Cd)Se/ZnSe asymmetric double quantum wells. Physical Review B. 1996;**53**:12637

[36] Hua J, Li-Gong Z, Zhu-hong Z, Anli-Nan, You-Ming L, Ji-Ying Z, et al. Temperature-Dependent Photoluminescence in Coupling Structures of CdSe Quantum Dots and a ZnCdSe Quantum Well. Chinese Physics Letters. 2005;**22**:1518-1521

[37] Saint-Girons G, Sagnes I. Photoluminescence quenching of a low-pressure metal-organic vapor-phase-epitaxy grown quantum dots array with bimodal inhomogeneous broadening. Journal of Applied Physics. 2002;**91**:10115

[38] Hall AC. A century of ellipsometry. Surface Science. 1969;**16**:1-13

[39] Rahmouni S, Zighed L, Tifouti I, Hadnine S, Aida MS. Experimental study of porous silicon films prepared on N and P type monocrystalline silicon wafers. Optoelectronics and Advanced Materials. 2017;**11**(1-2):105-108